Image Degradation due to Phase Effects in Chromeless Phase Lithography

Karsten Bubke[*1], Martin Sczyrba[1], KT Park[1], Ralf Neubauer[1], Rainer Pforr [2], Jens Reichelt [2], Ralf Ziebold [2]

[1]Advanced Mask Technology Center GmbH & Co. KG, Raehnitzer Allee 9, D-01109 Dresden, Germany

[2] Qimonda Dresden GmbH & Co. OHG, Koenigsbruecker Strasse 180, D-01099 Dresden, Germany

ABSTRACT

Chromeless Phase Lithography (CPL) is discussed as interesting option for the 65nm node and beyond offering high resolution and small Mask Error Enhancement Factor. However, it was shown recently that at high NA CPL masks can exhibit large polarization and also phase effects. A well known phase effect occurring for CPL semi dense lines are through focus Bossung tilts.
However, another manifestation of phase effects for dense lines and spaces is a reduced contrast for a symmetrical off-axis illumination due to phase errors between 0^{th} and 1^{st} diffraction order. In this paper it is shown that these phase effects can lead to a significant contrast loss for dense features smaller than 60nm half pitch. While also present for trench structures, the contrast reduction is more pronounced for mesa style structures. It is shown that for mesa structures an adjustment of etch depth can not recover an effective pi-phase shift. Furthermore, significant polarization effects are observed. As an example, the optimum mesa structure for TE polarization is shifted to small lines.
For an experimental validation, a CPL mask containing dense lines and spaces was fabricated. Their imaging performance was characterized with an AIMS 45i offering NA's greater than 1 and linearly polarized illumination as well as by wafer printing. Gratings with pitches down to 100 nm with varying duty cycles were measured with TE, TM and unpolarized dipole illumination. Very good agreement between measurement and simulation results confirmed the validity of theoretical predictions.

Keywords: Pellicle, Hyper NA Lithography, Aberration, Apodization, CD uniformity

1. INTRODUCTION

In the recent years various new techniques have been developed to further shrink the minimum feature sizes as requested by the semiconductor industry. The latest key innovations in optical lithography are immersion lithography and the introduction of polarized light. Since for the coming nodes mask feature sizes are in the order of the wavelength of the actinic light, topography effects on the mask need to be considered for the characterization of the mask performance. They may have severe impact on their lithographic performance and therefore need to be investigated carefully.
CPL masks have been studied for usage in advanced lithography since many years [1-7]. Main focus for application in the past was logic devices. But their lithographic potential has been extensively examined also for memory devices [8]. A specific advantage of this mask type to other phase-shifting masks is a very small mask error enhancement factor at comparable process window.
For mask strategy decisions it is important to know how mask topography and polarized light might impact the imaging performance and which place in lithography CPL masks might achieve in future lithography. The goal of this paper is the investigation of CPL masks with respect to their applicability for memory devices for sub-60nm half pitch. It will be shown that phase effects can lead to considerable image degradation which can not be compensated for by a simple adjustment of etch depth.

[*] karsten.bubke@amtc-dresden.com, phone +49 351 4048 377, fax +49 351 4048 9377

2. THEORY

In this paper we are interested in topography effects which arise while printing dense lines and spaces using CPL masks with off axis illumination. As sketched in Fig. 1, two scenarios for the actual mask layout are possible: mesa style structures and trench style structures.

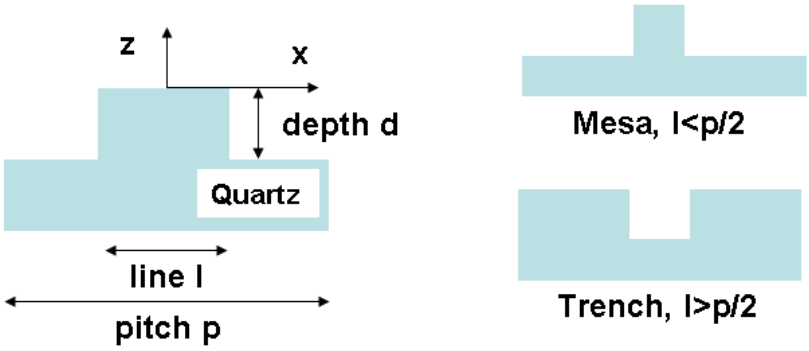

Figure 1: CPL mask: definition of geometry and coordinate system.

In what follows we will derive the essential effects of phase errors on image contrast by means of a simple model based on two beam interference assuming an ideal lens. Similar discussions can be found in, for example, [2, 9, 10]. Polarization dependent reflection at the resist surface as well as vector effects are neglected. This is a reasonable simplification when one considers immersion lithography in combination with polarized light. All rigorous simulations in this section are therefore performed with TE polarization. Mask polarization effects are addressed in the next section of this paper.

For dense structures near the resolution limit, only the 0^{th} and 1^{st} diffraction orders are captured by the entrance pupil of the lens and used to generate the aerial image. The intensity in resist due to a single source point (see Fig. 2) can then be written as [10, 11],

$$I(x) = |c_0|^2 + |c_1|^2 + 2|c_0||c_1|\cos\left(\frac{2\pi}{p}x + f(\phi_{\text{in}})z + \Delta\varphi\right), \quad \Delta\varphi = \arg(c_0) - \arg(c_1), \tag{1}$$

where c_0 and c_1 are the complex amplitudes of the respective diffraction orders and p is the pitch. Here and in the remainder of this paper the pitch and the line are given in wafer scale. Furthermore, according to the coordinate system sketched in Fig. 1, the relative phase of diffraction orders $\Delta\varphi$ is given at x=0, z=0. The function $f(\phi_{\text{in}})$ describes the printing behavior in defocus and is given by,

$$f(\phi) = \frac{2\pi}{\lambda}\left[\sqrt{n^2 - \left(\frac{\lambda}{p} - \sin\phi_{\text{in}}\right)^2} - \sqrt{n^2 - \sin^2\phi_{\text{in}}}\right], \tag{2}$$

where λ=193nm is the wavelength, ϕ_{in} is the illumination angle incident on the mask and n is the refractive index of the material between exit pupil of the projection lens and resist. In Eq. (2), the sine of the incident angle $\sin(\phi_{\text{in}})$ is multiplied by the reduction factor of the lens (M=4). From Eq. (1) it becomes clear that the created image is affected by both the magnitudes and phases of diffraction orders. However, the image contrast given by

$$\text{Contrast} = 2\frac{|c_0||c_1|}{|c_0|^2 + |c_1|^2}, \tag{3}$$

depends merely on the intensity of relevant orders. Maximum intensity modulation is obtained for |c0|=|c1|. A phase error $\Delta\varphi$ leads essentially to a focus dependent displacement which is also a function of the angle incident on the mask.

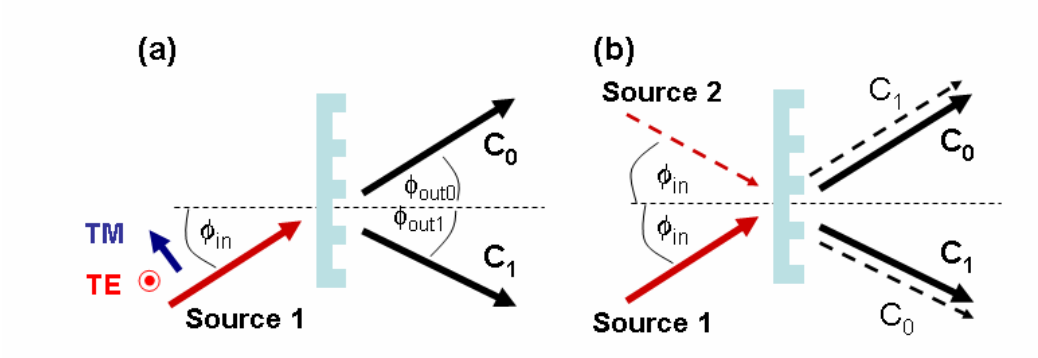

Figure 2: (a) illumination of dense lines and spaces with single source point (monopole) under an angle of incidence ϕ_{in} and respective 0^{th} and 1^{st} diffraction orders with complex amplitudes c0 and c1; (b) dipole illumination with two individual source points located symmetrically to optical axis.

As sketched in Fig. 2, the image tilt due to phase errors can be compensated for by an additional source point located symmetrically to the optical axis. The resulting intensity is an incoherent sum of the aerial images of individual source points. As phase errors for respective source points create displacements in opposite directions, the net shift is zero. The resulting intensity is given by ,

$$I(x) = |c_0|^2 + |c_1|^2 + 2|c_0||c_1|\cos\left(\frac{2\pi}{p}x\right)\cos\left[f(\phi_{in})z + \Delta\varphi\right], \tag{4}$$

whereas the intensity modulation is given by the contrast,

$$\text{Contrast} = 2\frac{|c_0||c_1|}{|c_0|^2 + |c_1|^2}\cos\left[f(\phi_{in})z + \Delta\varphi\right]. \tag{5}$$

For optimal dipole illumination, the angle of incidence is chosen in such a way that the diffraction orders leave the mask symmetrically to the optical axis ($\phi_{out0} = \phi_{out1}$). It can be shown that in this case $\sin\phi_{in} = \sin\phi_{opt} = \lambda/2p$ from which follows $f(\phi_{in}) = 0$. Hence, the aerial image has no focus dependence. As is evident from Eq. (5), phase errors lead to a reduction of contrast and hence to image degradation.

For angles different from optimal dipole illumination, the optimal image contrast experiences a focus shift. For a cone of angles around the optimal dipole, there is no net focus shift but still a reduction of contrast depending on the phase error between diffraction orders. Hence, optimum contrast not only requires the intensity in both diffraction orders to be equal but also the phase difference to be zero or 180°.

In the following we look at intensities and phase errors of relevant diffraction orders of dense lines and spaces of a CPL mask as sketched in Fig.1, in particular the differences between an infinitely thin mask (Kirchhoff mask) and a mask with topography. The diffraction pattern of a Kirchhoff mask can be calculated analytically. All topography simulations were performed by rigorous coupled wave analysis (RCWA) using the lithography simulator Prolith. It should be noted that for a correct description of the effects discussed here off-axis illumination is essential. The so called Hopkins approach, where the diffraction spectrum for oblique incidence is obtained by a simple shift of the spectrum for vertical illumination, leads to erroneous results in particular for structures smaller than 60nm half pitch [12,13].

Rigorous calculations were performed for half pitches of 75 and 50 nm (wafer scale), respectively. In Fig. 3, the ratio of the magnitudes $|c_0|/|c_1|$ as well as the phase difference $\arg(c_0)$-$\arg(c_1)$ of diffraction orders are plotted against the duty cycle (line/pitch) for optimal dipole illumination. Here, the etch depth for the topographical mask is the nominal depth for π phase shift $d = \lambda/2/(n_{Quartz}-1) = 171.4$nm.

Optimum contrast of a Kirchhoff mask is obtained for duty cycles of ~0.25 (mesa style) and ~0.75 (trench style). Whereas for mesa structures a phase difference of 180° is obtained, the phase difference for trench structures is zero. From Eq. (1) or (4) it is obvious that this corresponds to a change of polarity of the intensity distribution. As can be seen in Fig. 3, there are large differences in diffraction between Kirchhoff and topographical mask for small pitches. This applies to both the intensity and the phase of respective orders.

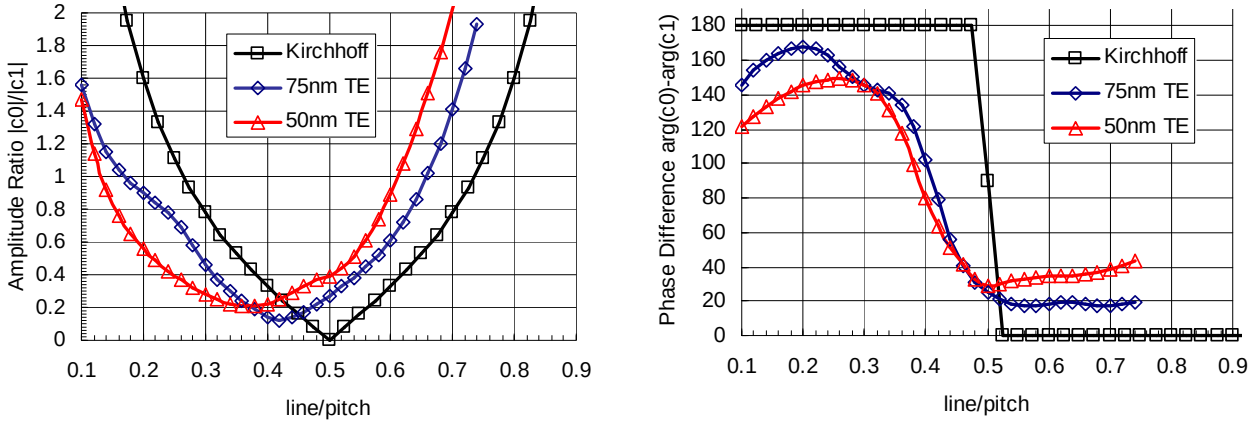

Figure 3: Ratio of magnitudes $|c_0|/|c_1|$ (left hand side) and phase differences $\arg(c_0)$-$\arg(c_1)$ (right hand side) of diffraction orders of infinitely thin mask (Kirchhoff mask) and a topographical mask (nominal etch depth d=171.4nm for π phase shift, optimal dipole, TE) for 50 and 75nm half pitch.

The impact of phase errors can be observed in Fig. 4, where the image contrast according to Eq. (3) and (5) is shown for optimal monopole and dipole illumination. For both mesa and trench structures a duty cycle exists for which the intensities in diffraction orders are equal. As a result, for one source point the effect of topography is merely a shift of optimal contrast to smaller duty cycles. The impact of phase errors becomes obvious for imaging of structures with 50nm half pitch using dipole illumination. Here, the maximum image contrast for both mesa and trench style structures is significantly smaller than for 75nm half pitch.

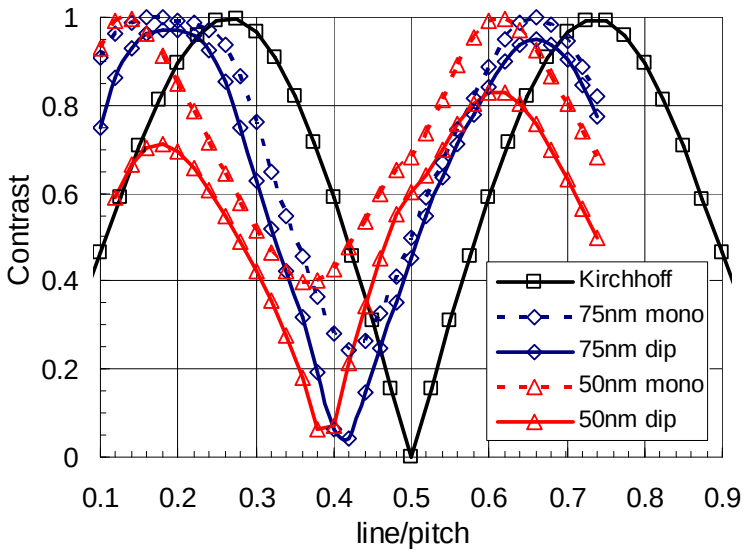

Figure 4: Image contrast for optimal monopole and dipole illumination according to Eq. (3) and (5), respectively (TE polarization, nominal depth for π phase shift $d=\lambda/2/(n_{Quartz}-1)=171.4$nm). Whereas for monopole illumination the optimum contrast is obtained for smaller duty cycles, the phase error leads to image degradation for dipole illumination.

Whereas the influence of mask topography on the magnitude of diffraction orders can be corrected for by simple biasing of the line or trench, a correction of the phase error requires an adjustment of etch depth. This is shown in Fig. 5 for structures with 75 and 50nm half pitch, respectively. The black lines correspond to structures with equal intensity $|c_0|^2=|c_1|^2$ in both diffraction orders. The red lines represent pattern with 0° or 180° phase difference. The blue lines correspond to structures with 90° or -90° phase difference in both orders resulting in zero contrast and hence complete image degradation. As stated earlier, a perfectly balanced structure is obtained if both optimum intensity and phase conditions can be achieved. Interestingly, this can be obtained for trench structures only. Here, with decreasing pitch the required etch depth increases to ~220nm for 50nm half pitch. For mesa style structures we find no simultaneous matching of both intensity and phase. Whereas for 75nm half pitch red and blue lines are still close to each other, the gap becomes significant for 50nm half pitch.

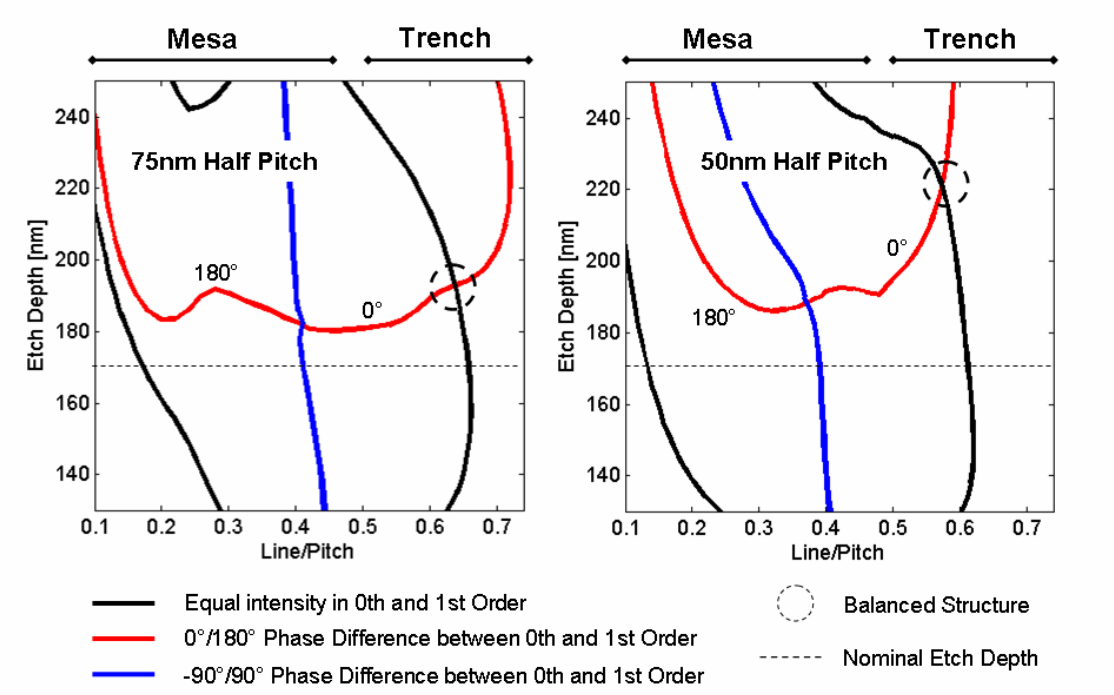

Figure 5: Contour plots for intensity and phase matching as a function of duty cycle and etch depth for 75nm and 50nm half pitch (TE polarization, optimal dipole); simultaneous balancing of intensity and phase is obtained for trench style structures only.

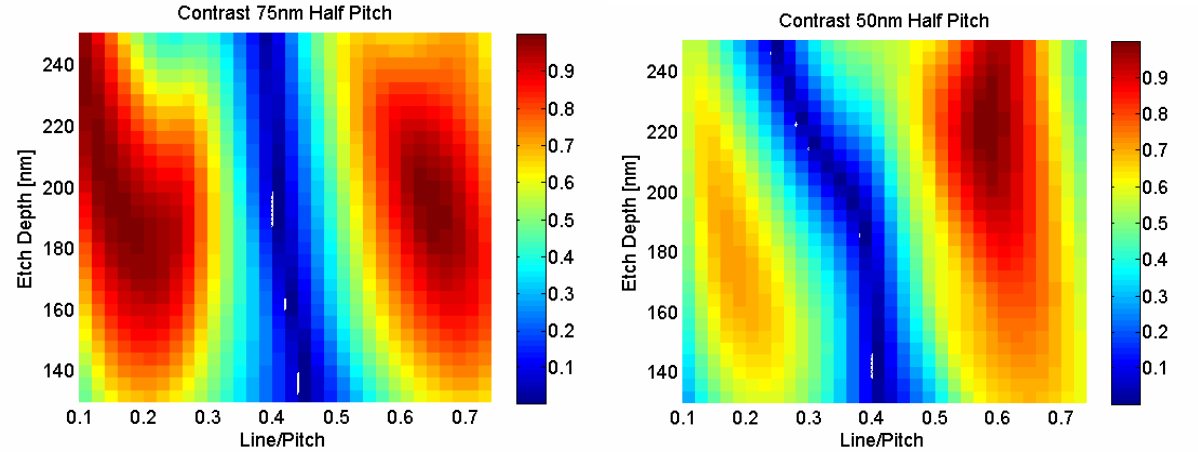

Figure 6: Image contrast for dipole illumination (TE) according to Fig. (5) for varying duty cycle and etch depth, respectively.

The impact of this mismatch between intensity and phase balancing is shown in Fig. 6, where the image contrast is plotted as a function of duty cycle and etch depth. For 75nm half pitch both mesa and trench style structures show areas with (near) optimum contrast 1. Required etch depths are in the order of 180-190nm. The situation is different for 50nm half pitch. Insufficient balancing of both intensity and phase leads to significant contrast and hence image degradation for mesa structures. An adjustment of etch depth can not compensate for this effect. Optimum trench structures require an etch depth of ~220nm and a trench width of ~160nm (mask scale) which might be difficult to process and control. Hence, the use of CPL structures for printing dense lines and spaces becomes challenging for small nodes.
It is interesting to look more closely at the evolution of contour lines as shown in Fig. 5 for decreasing pitch. This is depicted in Fig. 7. Also included here is a plot for a perfectly thin mask. For direct comparison with a topographical mask, phase errors from the nominal 180° were assumed which correspond to the etch depth plotted as *y*-axis.
The deviations from the behavior of a perfectly thin mask get larger with decreasing pitch. Whereas for 90nm half pitch both mesa and trench structures can be completely balanced, this is not possible for mesa structures for 75nm half pitch and below. However, as stated earlier, a significant effect on contrast can be observed for 65nm and below.

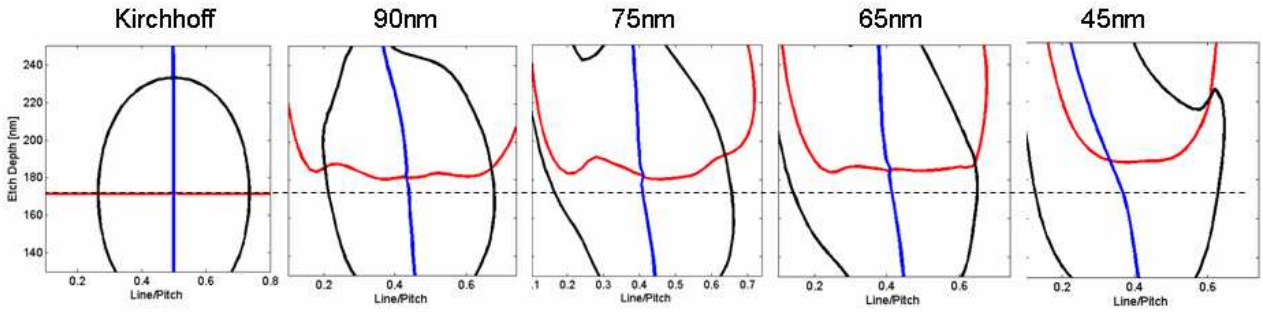

Figure 7: Evolution of contour lines for balanced structures according to Fig. 5 for varying pitches, also included is a comparison with a perfectly thin (Kirchhoff) mask, the dashed line corresponds to nominal etch depth; for half pitches smaller than 75nm mesa structures can not be balanced completely.

3. EXPERIMENTAL VERIFICATION

Measurement with AIMS 45i

After having discussed the impact of the phase differences between the diffraction orders we now focus on the experimental verification of this effect. For this purpose a CPL mask was manufactured containing arrays of lines and spaces with varying pitches and duty cycles. Used for the further evaluation were structures with a half pitch of 57.5nm and 50nm. The etch depth was approximately 183nm.
In a first step, the mask was exposed using an AIMS 45i tool with an NA=1.4 [14]. The illumination was a dipole centered on the optimal dipole setting for both pitches. The coherence was chosen to be $\sigma_{in}/\sigma_{out}=0.6$ with $\sigma_{out}=0.86$ for the half pitch of 50nm and $\sigma_{out}=0.75$ for the half-pitch of 57.5nm, respectively. Aerial images were taken using different states of polarization: TE, TM and unpolarized. No vector effect emulation was used.
Figs. 9 and 10 show the measured contrast for the two pitches as a function of duty cycle. In both plots the contrast was adjusted by a simple scaling to account for effects like flare and crosstalk [15]. For both pitches the contrast of the mesa structures is significantly smaller than for trench structures. This is in agreement with the findings discussed earlier in this study. Also obvious in Figs. 9 and 10 are large polarization effects. The phase errors for the structures considered here are larger for TM polarization. Optimal duty cycles for TE are obtained for smaller lines than for TM polarization. For comparison also the results of rigorous simulations are shown. The simulations are in good agreement with the experimental data.

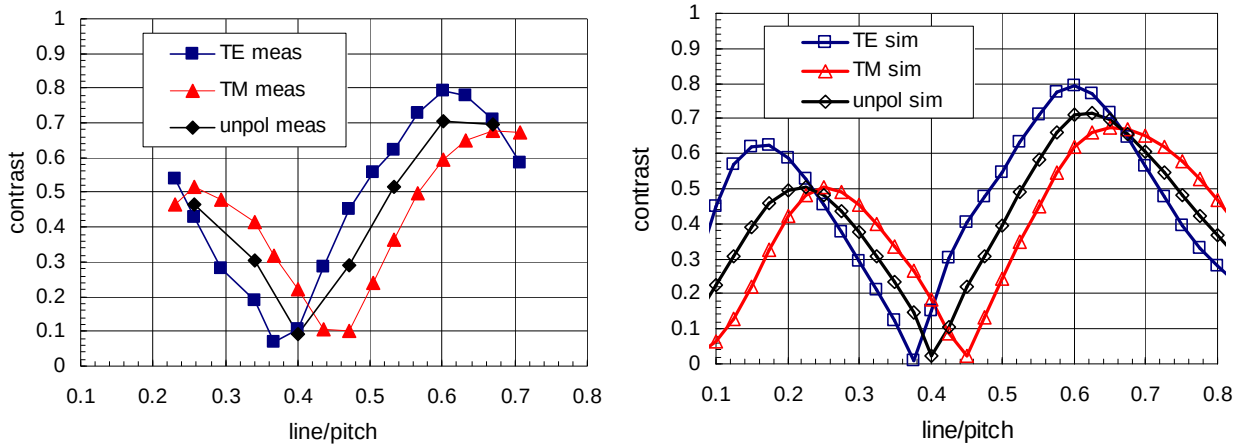

Figure 9: AIMS measured contrast (left) versus duty cycle for a CPL mask with half pitch 50nm compared to simulation results (right).

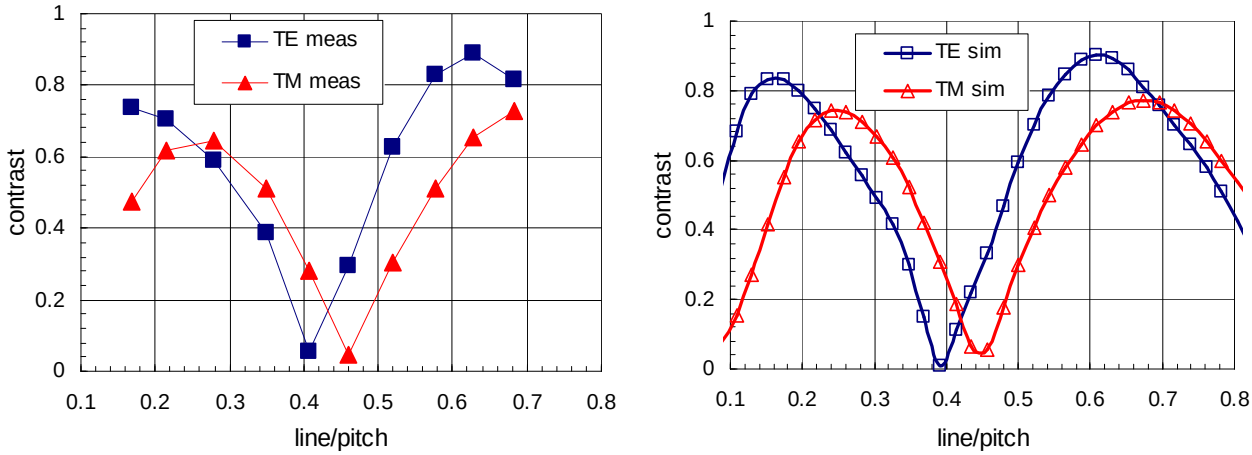

Figure 10: AIMS measured contrast (left) versus duty cycle for a CPL mask with half pitch 57.5nm compared to simulation results (right).

Wafer Prints

To verify the simulation results described above also wafer prints have been performed. As measure of the aerial image contrast exposure latitude (EL) at nominal focus can be chosen. Also structural depth-of-focus (DOF) is applicable as criterion, since line collapsing occurs at a specific critical contrast limit in defocus (far before a ten percent CD deviation criterion is violated).

57.5nm half pitch gratings have been used for the experiments, since they are close to the resolution limit of the largest dry NA (0.93) of the available projection systems. For the imaging dipole illumination with 0.97 outer and a 0.82 inner sigma has been applied in conjunction with TE polarized and unpolarized light. For good technical reasons TM polarization is not available in conjunction with dipole illumination at scanners. An advanced 193nm resist process with a layer thickness close to 170nm has been used for pattern print.

Figure 11 shows the EL and DOF versus the line-pitch ratio for TE polarization. Furthermore SEM pictures are implemented in the graph to demonstrate the DOF differences at the extremes of the curves. Both curves show the expected modulation across the line-pitch ratio. Curve maxima are observed for line-pitch ratios of 0.26 (mesa) and 0.60

(trench), which are very close to the values obtained from simulation and AIMS measurements. Trench features seem to give a somewhat larger DOF and EL than mesas. Almost no image contrast is obtained at a line-pitch ratio of 0.413, which also fits well to the results above.
For unpolarized light (Figure 12) basically the same trend can be observed, but compared to the results for TE polarization the process window is severely degraded. This is mainly due to the vector effects within the resist, which result in a degradation of the image contrast of the TM components of the incident un-polarized light. Note that the AIMS system does not show this degradation due to constructive deviation to a lithographic lens (the image is magnified instead of de-magnified like in the scanner projection system, i.e. the AIMS causes much smaller incident angles between the interfering beams). In summary it can be concluded, that the wafer print results verify fairly well the performance suggested by simulations.

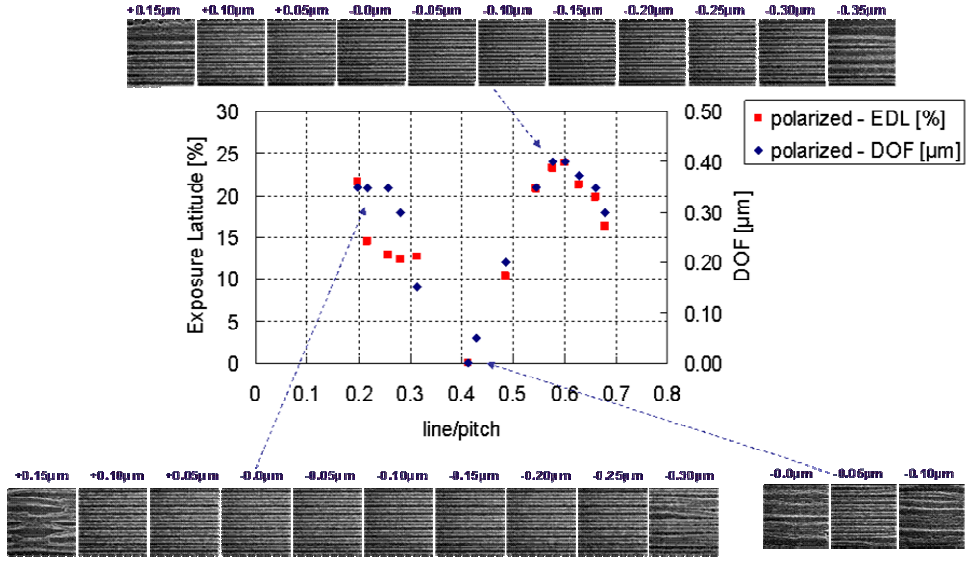

Figure 11: EL and DOF of 57.5nm lines-spaces versus the line-pitch ratio for TE polarization.

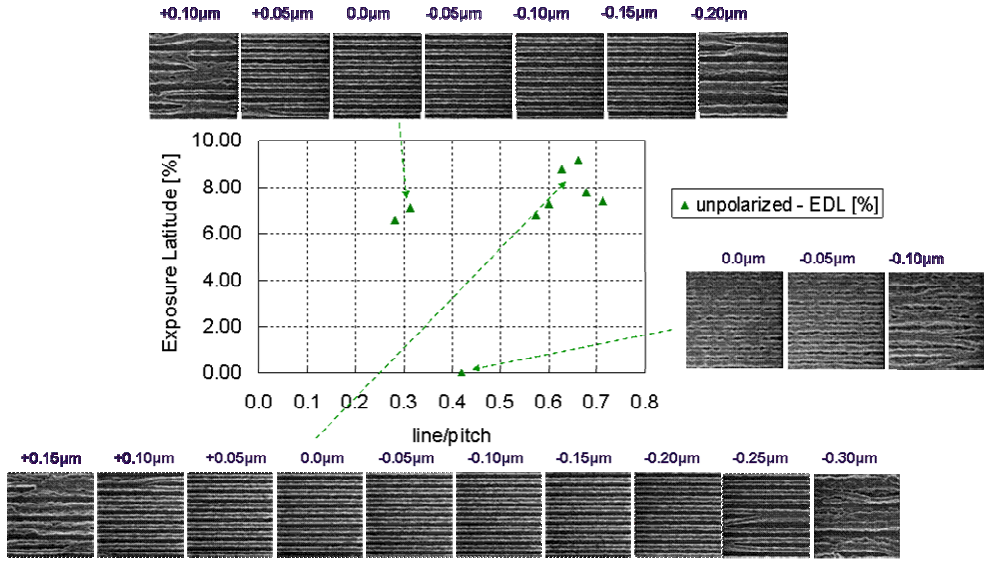

Figure 12: EL and DOF of 57.5nm lines-spaces versus the line-pitch ratio for unpolarized light.

4. CONCLUSIONS

The purpose of the present study was to investigate the lithographic potential of CPL masks for memory devices for future feature shrinks. To do so simulation and experimental investigations have been performed for the 60nm node and below. Differences in the phases of the diffraction orders lead to a degradation of the image quality mainly for mesa style CPL masks. The contrast reduction increases for decreasing half pitch. For trench structures the phase effect can be compensated for by an adjustment of the etch depth. This adjustment is not possible for mesa structures for half pitches smaller than ~75nm and below. This implies that trench structures are preferable for printing of dense lines and spaces. The theoretical predictions have been verified by experiments.

ACKNOWLEDGEMENTS

AMTC is a joint venture of Infineon, AMD and Toppan Photomasks and gratefully acknowledges the financial support by the German Federal Ministry of Education and Research (BMBF) under Contract No. 01M3154A ("Abbildungsmethodiken für nanoelektronische Bauelemente"). The authors would like to thank Andrew Ridley and Ulrich Stroeßner from Carl Zeiss SMS GmbH for help with the AIMS measurements and Andreas Erdmann from Fraunhofer IISB Erlangen for useful discussions.

REFERENCES

[1] M. Hsu, et al, "RET Masks for Patterning 45nm Node Contact Hole Using ArF Immersion Lithography", *Proceedings of the SPIE*, vol. 6283, 6283217-1, 2006.

[2] J. Bekaert, et al, "Compensating mask topography effects in CPL through-pitch solutions toward the 45nm node", *Proceedings of the SPIE*, vol. 5992, 59921O, 2005.

[3] V. Philipsen, et al, "Mask Topography effects in chromeless phase lithography", *Proceedings of the SPIE*, vol. 5567, pp. 669-679, 2004.

[4] Y. F. Cheng, et al, "The investigation of 193nm CPL 3D Topology Mask Effect on Wafer Process Performance", *Proceedings of the SPIE*, vol. 6154, 61542D-1, 2006.

[5] Y. Kojima, et al, "Performance Study of Chromeless Phase Lithography Mask for the 65nm Node and Beyond", *Proceedings of the SPIE*, vol. 6154, 615428-1, 2006.

[7] T. Adachi, et al, "Lithographic performance comparison with various RET for 45nm node with hyper NA", *Proceedings of the SPIE*, vol. 6283, 62832W-1, 2006.

[8] R. Pforr, et al, "Hard phase shifting masks for the 65nm node – A performance comparison", *Proceedings of the SPIE*, vol. 5377, pp. 212-221, 2004.

[9] C. A. Mack, M. D. Smith, and T. Graves, "The impact of attenuated phase shift mask topography on hyper-NA lithography", *Proceedings of the SPIE*, vol. 5992, 2005.

[10] J. Cobb, et al, "The impact of mask topography on CD control", *Proceedings of the SPIE*, vol. 5754, pp. 395-406, 2005.

[11] A. K. Wong, "Resolution Enhancement Techniques in Optical Lithography", SPIE Press, 2001.

[12] A. Erdmann, P. Evanschitzky, and P. De Bisschop, "Mask and Wafer Topography Effects in Immersion Lithography", *Proceedings of the SPIE*, vol. 5754, pp. 383-394, 2005.

[13] J. Schermer, P. Evanschitzky, and A. Erdmann, "Rigorous Mask Modeling beyond the Hopkins Approach", *Proceedings of the SPIE*, vol. 6281, 2006.

[14] A. Zibold, et al, "First results for hyper NA scanner emulation from AIMS^{TM} 45-193i", *Proceedings of the SPIE*, vol. 6283, 628312, 2006.

[15] Teuber, I. Higashikawa, J.-P. Urbach, C.M. Schilz, R. Koehle, A.M. Zibold, "First results from AIMS beta tool for 157nm lithography", *Proceedings of the SPIE*, vol. 5377, 2004.